Invited Paper

Optoelectronic properties and characteristics of doping superlattices

V.K. Kononenko, I.S. Manak, and D.V. Ushakov

Stepanov Institute of Physics, National Academy of Sciences of Belarus
Fr. Scorina Pr., 70, 220072 Minsk

ABSTRACT

Optical and electric properties of doping superlattices, or n-i-p-i crystals, can be varied in a wide range under excitation and through the choice of the thicknesses and doping of the crystal layers. Some basic results concerned the transformation of the electron energy spectrum of doping superlattices are summarized. Parameters and characteristics of doping superlattices related to optoelectronics devices, such as photodetectors, laser diodes, and optical modulators, are presented.

Keywords: doping superlattices, potential relief, energy spectrum, density of states, screening, diffusivity-mobility ratio, δ-doping, light absorption, spontaneous emission, gain

1. INTRODUCTION

1.1. Historical aspects

A fundamental idea of the superlattice effect was expressed in 1962. [1] When electrons of a crystal are in the field of standing ultrahigh-frequency sound waves, an additional periodic potential appears that results in the formation of minibands in the electron energy spectrum. Technology principals to produce an additional periodic potential in semiconductors were described at first in 1970. [2] Two types of superlattices with compositional and doping structures have been introduced. Early realization of doping superlattices such as periodic p-n-p-n structures in Si was carried out in the Soviet Union. [3] In that period, compositional superlattices in the GaAs-GaP system were produced by gas epitaxy. [4,5] One modification of doping superlattices is δ-doping superlattices. A theory of this type superlattices was presented in Ref. 6 and the term "n-i-p-i crystals" was suggested as well. The method of molecular beam epitaxy was used to grow superlattices in the GaAs-AlGaAs system. [7] Afterwards, this modern technology was used to receive n-i-p-i structures in GaAs with the dopants Be and Si. [8] Before long, laser effect was achieved. [9] And at last, the introducing of heterostructures in doping superlattices has been proposed. [10] These structures find good characteristics for the detecting and modulation of optical signals. [11]

Comprehensive reviews of properties of compositional and doping superlattices can be found in Refs. 12-16. In compositional superlattices, there are two main types structures with different band alignments (Fig. 1). Some additional modifications of compositional and doping superlattices exist. One of the most interesting variations of compositional superlattices is superlattices based on asymmetric multiple quantum-well heterostructures. [17] These structures consist of semiconductors layers of different thicknesses and/or alloy compositions (Fig. 2). It gives a new freedom to widen functions of optoelectronic devices, in particular, to receive a broad-band spectrum of amplification of radiation. [18,19]

Another way to obtain a staggered band alignment, similar to the type II compositional superlattices, is the introducing of different impurities to a bulk specimen (n-i-p-i crystals) (Fig. 3). When using δ-mode of dopant deposition, superlattices with the sawtooth potential profile occur (Fig. 4(a)). Asymmetric structures are also possible in doping superlattices. [20,21] E.g., δ-doped superlattices with different thicknesses of i-layers between donor and two adjacent acceptor planes have asymmetric potential profiles (Fig. 4(b)). Periodic grading the composition of ternary or quaternary semiconductors during growth allows to obtain graded-gap superlattices. In such structures easily to reach an avalanche process and receive the solid-state photomultiplier regime. [22] Inserting additional quantum wells in compositional and doping superlattices gives possibilities to control overlapping electron and hole wave functions and change specific optoelectronic parameters and characteristics.

1.2. Features of doping superlattices

Doping superlattices, or n-i-p-i crystals, belong to a novel type of semiconductor optoelectronics elements. Optical and electric properties of doping superlattices can be varied in a wide range under excitation and through the choice

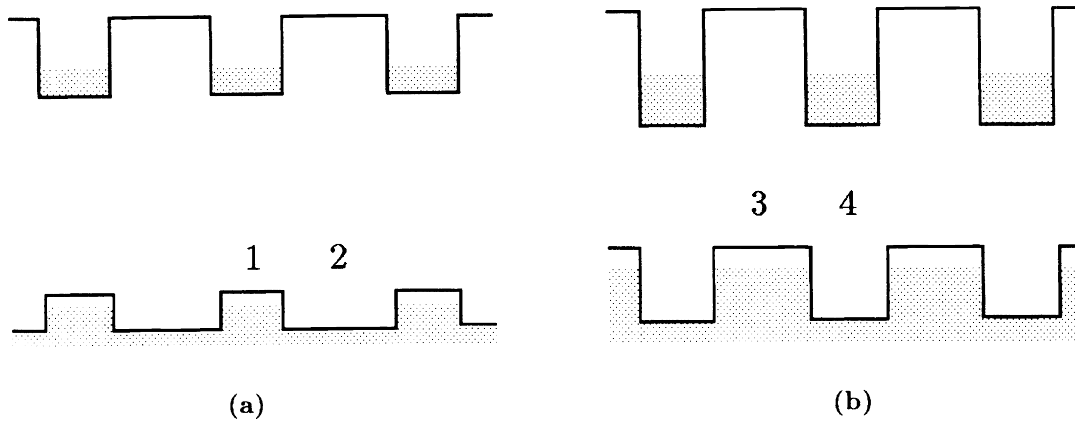

Fig. 1. Schematic energy band diagrams of compositional (a) type I and (b) type II (or staggered alignment) superlattices. Possible pair semiconductor materials are (1) GaAs, (2) AlGaAs, (3) GaSbAs, (4) GaInAs. States filled by electrons are marked by points.

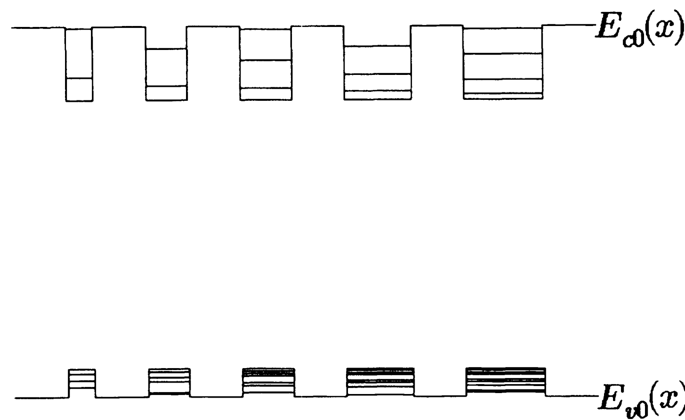

Fig. 2. Band diagram of an asymmetric five quantum-well heterostructure in the GaAs-$Al_xGa_{1-x}As$ system. In the quantum wells, subband levels of electrons and holes are shown. Energies at the bottom of the conduction band $E_{c0}(x)$ and at the top of the valence band $E_{v0}(x)$ depend on the Al mole fraction x.

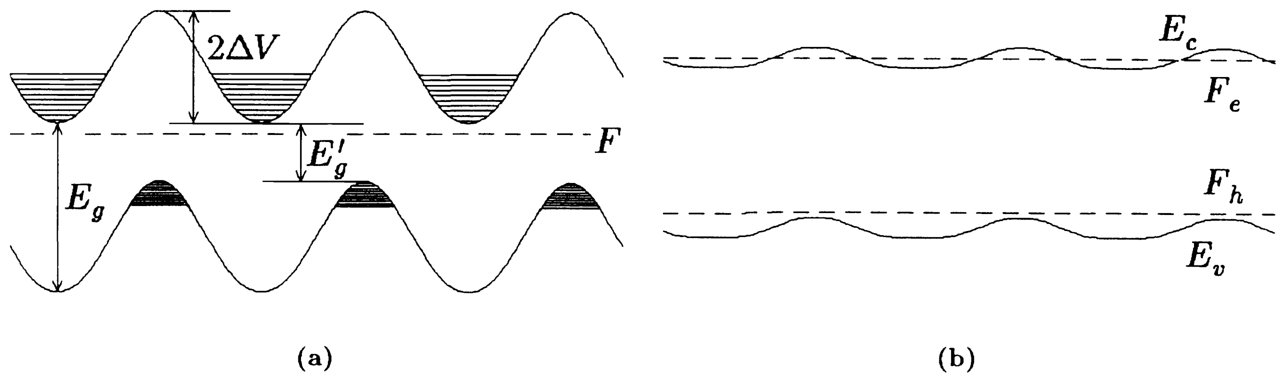

Fig. 3. Band diagrams of an n-i-p-i crystal (a) at the thermodynamical equilibrium and (b) under excitation. F is the Fermi level, E_g is the energy band gap of the host semiconductor, E_g' is the effective energy band gap of the superlattice, $2\Delta V$ is the depth of the potential relief, F_e and F_h are the quasi-Fermi levels for electrons and holes. Subband levels in the potential profile parabolic parts are shown too. E_c and E_v are the energies of electron and hole states.

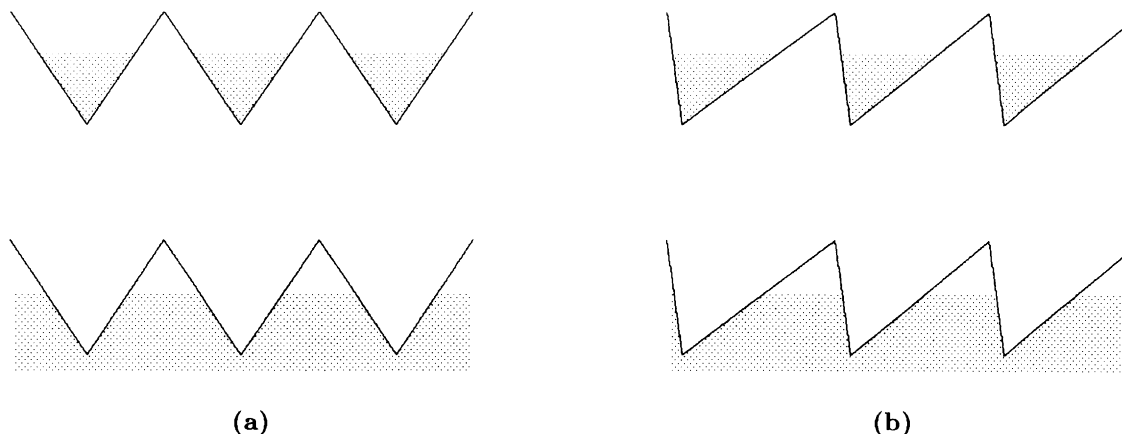

Fig. 4. Band diagrams of doping superlattices with δ-doped (a) symmetric and (b) asymmetric structures.

of the thickness and doping of the crystal layers. The main features of doping superlattices are (1) spatial separation of electrons and holes in different remote quantum wells, (2) tunable energy band gap under optical or electric excitation, (3) increased current carrier lifetime and smaller oscillator strength of optical transitions as compared to bulk materials, (4) strong changing energy level structure in dependence on doping impurities distribution and concentrations of donors and acceptors, and (5) wide possibilities to vary optical properties and characteristics due to design parameters or introducing additional quantum wells and using δ-doped regions.

In the paper, optoelectronic parameters and characteristics of doping superlattices are considered and some problems related to photodetectors, laser sources, and optical modulators are presented. In the beginning, some basic results about the electron energy structure of n-i-p-i crystals are summarized. Different approximations for the determining of the potential relief in doping superlattices are discussed and data of self-consistent calculations of the Schrödinger and Poisson's equations are presented. Transformation of electron energy levels, wave functions and spectra of absorption and emission of doping superlattices under excitation is examined in detail. The character of changing the overlap integrals of electron and hole wave functions and mechanisms of optical transitions in doping superlattices at different pump and doping levels are described. In conclusion, necessity to optimize parameters and characteristics of optoelectronic devices based on doping superlattices is marked.

2. POTENTIAL PROFILE AND ENERGY SPECTRUM

2.1. Approaches for the determining of the potential relief

The energy spectrum and optoelectronic characteristics of doping superlattices are determined by the potential energy profile. To find the potential relief in a doping superlattice, it is necessary to solve Poisson's equation. The potential energy profile depends on the thicknesses of the n- and p-type layers d_n and d_p, the donor and acceptor concentrations N_d and N_a, the undoped i-layer thickness d_i, and the concentrations of nonequilibrium current carriers.

Usually, the so-called effective width approximation is used to describe the superlattice potential $V(z)$ which includes flat and linear neutral parts and parabolic sections in between. [23,24] This approach is rather well suitable at low temperatures and for the large superlattice period $d = d_n + d_p + 2d_i$. The effective widths of space charge regions are

$$2d_n^+ = d_n\left(1 - \frac{n}{N_d d_n}\right) = d_n(1-r), \quad 2d_p^- = d_p\left(1 - \frac{p}{N_a d_p}\right) = \frac{N_d}{N_a} d_n(1-r). \tag{1}$$

Here, n and p are the sheet concentrations of electron and holes, respectively, $r = n/N_d d_n$ is the pump factor. From the condition of the macroscopic electroneutrality of the structure follows the equality $p = n + N$, where $N = N_a d_p - N_d d_n$. For compensated ($N = 0$) or p-type ($N > 0$) superlattices, the factor r changes from nearly 0 up to 1 at increasing the excitation. The potential profile depth is represented as follows

$$2\Delta V = \frac{\pi e^2}{\epsilon} N_d d_n \left(2d_i + \frac{N_a + N_d}{2N_a} d_n\right)(1-r)\left(1 - \frac{r}{1 + \frac{2N_a}{N_a + N_d}\cdot\frac{2d_i}{d_n}}\right), \tag{2}$$

where ϵ is the static dielectric constant of the semiconductor.

For structures with short periods and at room and higher temperatures, an approximation of effective concentrations of ionized impurities more suitable as a first step to find the potential relief. It is convenient to introduce the effective concentrations of ionized impurities in the form [25]

$$N_d^+ = N_d - \frac{n}{d_n} = N_d(1-r), \quad N_a^- = N_a - \frac{p}{d_p} = N_d\frac{d_n}{d_p}(1-r). \tag{3}$$

The solution of Poisson's equation in this approximation gives the electrostatic potential in n- and p-layers to be parabolic (without flat intervals) and independent on the ratio between the impurities concentrations. In this case, the potential relief depth

$$2\Delta V = \frac{2\pi e^2}{\epsilon}\left[N_d^+\left(\frac{d_n}{2}\right)^2 + N_a^-\left(\frac{d_p}{2}\right)^2 + N_d^+ d_n d_i\right] \tag{4}$$

varies linearly with r. For the p-type and compensated superlattices ($N \geq 0$), one finds

$$2\Delta V = \frac{\pi e^2}{\epsilon}\cdot\frac{N_d d_n}{2}(d + 2d_i)(1-r). \tag{5}$$

An analogous expression can be obtained for the n-type structure ($N < 0$) if in Eq. (5) to replace n by p and $N_d d_n$ by $N_a d_p$. As follows from comparison of Eqs. (2) and (5), Eq. (5) gives a larger value of $2\Delta V$ than Eq. (2). The values of $2\Delta V$ according by Eqs. (2) and (5) are coincident, obviously, only at $r = 1$ and for a compensated superlattice at $r = 0$.

It is evident that for the noncompensated superlattice, when $N_a d_p \neq N_d d_n$, the mixed approximation can be used. In this case, for more high doping parts of the structure, it is expedient to use the approximation of the space charge effective width and, for less doping parts, the approximation of the effective concentration of ionized impurities. For example, for the p-type structure ($N > 0$), the effective concentration of ionized donors in the n-layer $N_d^+ = N_d(1-r)$ and the effective width of the negative space charge region $2d_p^- = (N_d d_n/N_a)(1-r)$ in the p-layer are introduced. Then, from Poisson's equation one easily finds the potential relief and its depth

$$2\Delta V = \frac{\pi e^2}{\epsilon} N_d d_n \left(2d_i + \frac{N_a + N_d}{2N_a} d_n\right)(1-r)\left(1 - \frac{r}{1 + \frac{N_a}{N_d}\left(1 + \frac{4d_i}{d_n}\right)}\right). \tag{6}$$

As is seen, at $r = 0$ the values of $2\Delta V$ determined from Eqs. (2) and (6) are coincident, and at $r > 0$ Eq. (6) gives the value of $2\Delta V$ that is intermediate between the quantities given by Eqs. (2) and (5).

At the sufficiently high excitation power, when $r \geq 1$, the potential relief follows modulated concentration of nonlocalized current carriers. In this case, the approach of the bulk carriers distributed periodically in the z-axis direction of the superlattice can be used, [25] i.e.,

$$n(z) = \frac{n}{d} + A_n \cos(\frac{2\pi z}{d}), \qquad p(z) = \frac{p}{d} - A_p \cos(\frac{2\pi z}{d}). \tag{7}$$

Here, A_n and A_p are the coefficients defined by the energy band parameters and excitation level of the semiconductor. The potential profile depth is as follows

$$2\Delta V = \frac{\pi e^2}{2\epsilon}\left(N_a d_p(d-d_p) + N_d d_n(d-d_n)\right) - \frac{2e^2}{\pi\epsilon}\left(A_n + A_p\right) d^2. \tag{8}$$

At high levels of excitation, when the semiconductor becomes degenerated, for a compensated superlattice the value of $2\Delta V$ varies as $r^{-1/3}$. Comparison of different approaches for the potential profile depth versus the excitation level is shown in Fig. 5.

In the general case, the self-consistent solution of the Schrödinger and Poisson's equations should be carried out. The used equation system in the effective mass approximation has the form

$$\nabla^2 V(z) = \frac{4\pi e^2}{\epsilon}\left(p(z) - n(z) - N_a(z) + N_d(z)\right), \tag{9}$$

$$\begin{aligned} &\left[-\frac{\hbar^2}{2m_c}\nabla^2 + V(z)\right]\psi_{cn\nu}(z) = E_{cn\nu}\psi_{cn\nu}(z), \\ &\left[-\frac{\hbar^2}{2m_{vi}}\nabla^2 + 2\Delta V - V(z)\right]\psi_{vim\nu}(z) = E_{vim\nu}\psi_{vim\nu}(z), \end{aligned} \tag{10}$$

$$\begin{aligned} n(z) &= N_{c1}\sum_n\sum_\nu \ln\left(1 + \exp\frac{F_e - E_{c0} - E_{cn\nu}}{kT}\right)|\psi_{cn\nu}(z)|^2, \\ p(z) &= \sum_i N_{vi1}\sum_m\sum_\nu \ln\left(1 + \exp\frac{E_{v0} - E_{vim\nu} - F_h}{kT}\right)|\psi_{vim\nu}(z)|^2, \end{aligned} \tag{11}$$

where $N_{c1} = m_c kT/\pi\hbar^2 N_p$ and $N_{vi1} = m_{vi} kT/\pi\hbar^2 N_p$ are the sheet effective densities of states for electrons and heavy $(i = h)$ and light $(i = l)$ holes with the corresponding effective masses m_c and m_{vi}, N_p is the number of superlattice periods, T is the temperature, F_e and F_h are the quasi-Fermi levels for electrons and holes. One from bottoms of the potential wells in the conduction band is connected with zero value of the z-coordinate. The energy of the bottom of the conduction band in this point is denoted E_{c0}. And the top of the valence band through a halfperiod (at $z = d/2$) is E_{v0}. Therefore, the effective energy band gap of the superlattice equals to $E_g^{'} = E_{c0} - E_{v0} = E_g - 2\Delta V$, where E_g is the energy band gap of the host semiconductor. Values $E_{cn\nu}$ and $E_{vim\nu}$ are the dimensional quantization level energies, $\psi_{cn\nu}$ and $\psi_{vim\nu}$ are the envelope wave functions in the conduction and valence bands for the subbands with the quantum numbers n and m, respectively, and for the minisubbands with the quantum number ν. The wave functions are normalized on 1 per a period of the superlattice.

It is obvious that the potential relief and energy spectra in the quantum wells for electrons and holes subject to influence of many-body effects such as exchange and correlation interactions. The exchange-correlation term of the potential can be evaluated in the local density approximation of the density functional formalism. [26] The resulting band-gap renormalization corrections are more significant at high excitation of quantum-well systems. [27] Additional effects arise in doping superlattices due to the random distribution of the impurity dopants, first at all, the appearance of a density of states which exhibits tails.

The calculations for the GaAs doping superlattices show that, although the space charge distributions can be marked different in the mentioned above approximations, the potential relief remains practically the same. Distributions of

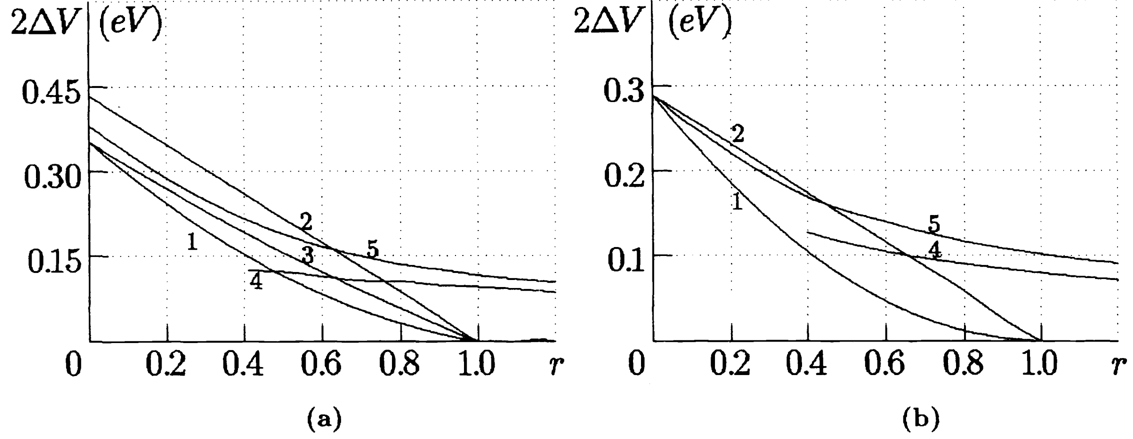

Fig. 5. Potential profile depth $2\Delta V$ versus the pump factor r, (1) the effective width approximation, (2) effective impurity concentration approximation, (3) mixed approximation, (4) modulated bulk carrier concentration approach, (5) self-consistent calculation for the GaAs (a) p-type and (b) compensated superlattices. (a) $N_a = 8 \times 10^{18}$ cm^{-3}, $N_d = 4 \times 10^{18}$ cm^{-3}, $d_p = d_n = 15$ nm, $d_i = 2.5$ nm, (b) $N_a = N_d = 8 \times 10^{18}$ cm^{-3}, $d_p = d_n = 10$ nm, $d_i = 0$, $T = 300$ K.

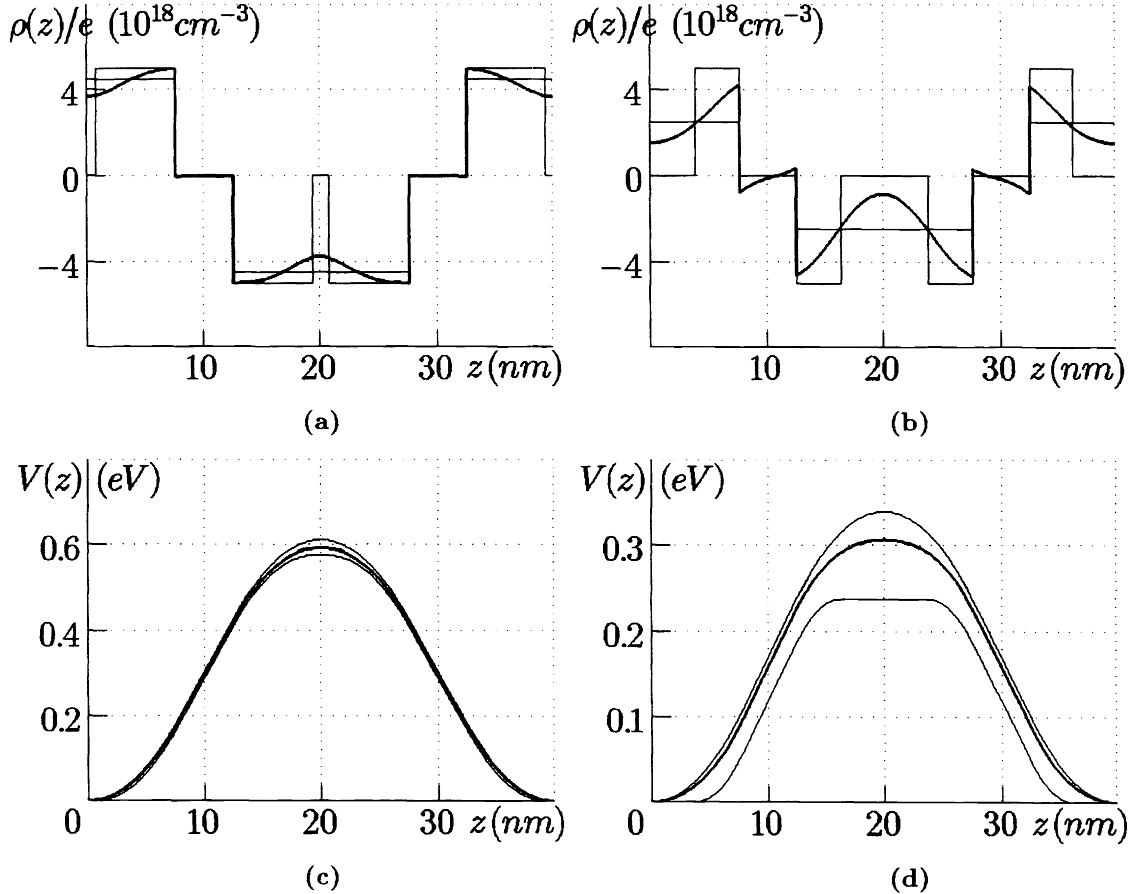

Fig. 6. (a), (b) Charge density distributions $\rho(z)$ and (c), (d) potential profiles $V(z)$ at different r. $N_a = N_d = 5 \times 10^{18}$ cm^{-3}, $d_p = d_n = 15$ nm, $d_i = 5$ nm, $T = 300$ K. (a), (c) $r = 0.1$, (b), (d) $r = 0.5$. Solid curves correspond to the effective width and impurity concentration approximations. Heavily drawn curves give results of self-consistent calculations.

the charge density calculated in different approximations are shown in Fig. 6. At an arbitrarily low excitation level the flat intervals, appeared in the central parts of the doped layers according to the effective width approximation, are not markedly manifested and potential shapes obtained in different approximations are close to the true relief. With increasing the pump r the results in the effective width approximation begin noticeably to differ from the self-consistent potential calculations, and the effective impurity concentration approach is more preferable. The approximation of the effective concentrations of ionized impurities or the mixed approximation give both the potential relief form and the depth $2\Delta V$ that are the most close to the exact self-consistent data. The calculated potential energy profiles for typical n-i-p-i crystals are in agreement with the results of direct measurements of the electrostatic potential spatial distribution by the scanning microscopy method. [28]

2.2. Electron energy levels and wave functions

The electron energy eigenstates in the n-i-p-i structure are found from the solving of the Schrödinger equation. In the effective mass approximation, since the superlattice potential $V(z)$ is periodical in the z-axis direction, the envelope wave functions are presented in the form $\psi(z) = \varphi(z)\exp(ik_z z)$. Then, the Schrödinger equation reduces to the differential equation

$$\frac{d^2\varphi(z)}{dz^2} + 2ik_z\frac{d\varphi(z)}{dz} + \left[\frac{2m}{\hbar^2}(E - V(z)) - k_z^2\right]\varphi(z) = 0. \tag{12}$$

Here, for simplicity subscripts at ψ, φ, m and E are omitted. As the crystal has finite dimensions, the function $\psi(z)$ satisfies the Born-Karman cyclic condition, i.e., $\psi(z) = \psi(z + N_p d)$. Then, one obtains $k_z = 2\pi\nu/N_p d$, where $\nu = 0, 1, .., N_p - 1$. So, the energy spectrum includes minisubbands (Fig. 7). In view of the potential symmetry therewith, the number of levels in a minisubband is equal to $N_p/2 + 1$ for even N_p and $(N_p + 1)/2$ for odd N_p. It is obvious that the states with the quantum numbers ν and $N_p - \nu$ correspond to the same energy eigenvalues, the envelope wave functions for these states are comprehensively conjugate. Evident also, the same conclusions are obtained when the momentum space is reduced to the first Brillouin zone $-\pi/d \le k_z \le \pi/d$. The envelope wave functions $\psi(z)$ are even (odd) in every well and also even from well to well in the Brillouin zone center ($k_z = 0$) when the subband quantum number n is even (odd) (Fig. 8 (a)). At the edges of the Brillouin zone ($k_z = \pm\pi/d$) the functions $\psi(z)$ are even (odd) in every well but odd from well to well when the quantum numbers n are even (odd) (Fig. 8 (b)). The value $k_z = 0$ corresponds to the minimum energy in minisubbands for every even-number subband and to the maximum energy in minisubbands when n is odd.

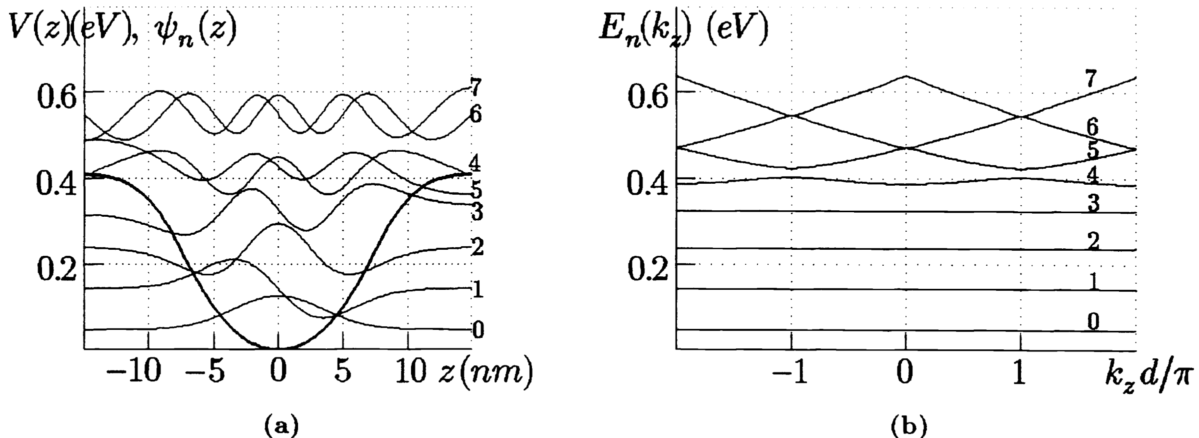

Fig. 7. (a) Potential relief $V(z)$ and wave functions for electrons $\psi_n(z)$ at $k_z = \pi/d$ and (b) energy dispersion $E_n(k_z)$. Figures denote the quantum numbers n of the subbands. $N_a = 10^{19}$ cm^{-3}, $N_d = 6 \times 10^{18}$ cm^{-3}, $d_p = d_n = 15$ nm, $d_i = 0$, $r \approx 0$. The wave functions are shown in the arbitrary unit scale.

Eq. (12) was solved by a numerical method. The derived energy dispersion $E_n(k_z)$ and the wave functions $\psi_n(z)$ for electron subbands with the quantum numbers n in specific points of the Brillouin zone are shown in Figs. 7 and 8. As seen, a considerable width of minisubbands occurs at the subbands with energies greater than $2\Delta V$. So, the filling of the subband levels in the n-i-p-i crystal quantum wells by nonequilibrium current carriers leads, in response

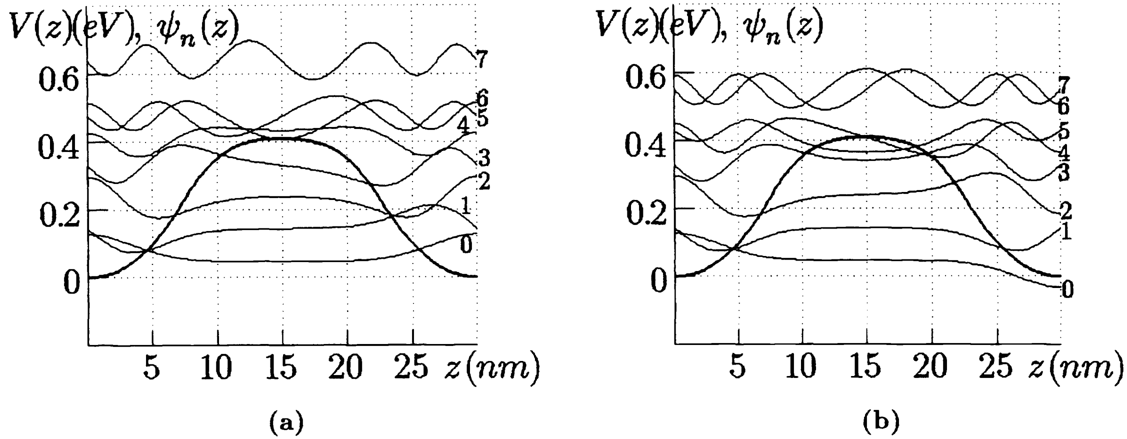

Fig. 8. Potential relief $V(z)$ (heavily drawn curves) and envelope wave functions $\psi_n(z)$ for electrons at (a) $k_z = 0$ and (b) $k_z = \pi/d$. Figures denote the quantum numbers of the subbands n. $N_a = 10^{19}$ cm^{-3}, $N_d = 6 \times 10^{18}$ cm^{-3}, $d_p = d_n = 15$ nm, $d_i = 0$, $r \approx 0$.

to the spatial charge redistribution, to the change of the electrostatic potential profile, which is accompanied by transformation of the dimensional quantization levels themselves, decrease of the quantum well depth and growth of the effective band gap.

3. ACCOUNT OF THE FLUCTUATED IMPURITY CHARGE POTENTIAL

3.1. Tails of the density of states

At high levels of doping of a semiconductor the energy spectrum of current carriers changes. [29] Because of overlapping the impurity band with the nearest intrinsic band of the crystal, the tail of the density of states appears. Account of the tails is important for interpretation of electric and optical phenomena in doped semiconductors. In particular, in spectra of absorption, gain, and luminescence of the structures based on doping superlattices a significant long-wavelength tail is observed. [30] Taking into consideration the fluctuations of impurity concentrations gives an opportunity to explain the experimental data.

To determine the density of states in doping superlattices, the method developed for the heavily doped bulk semiconductors will be used. [31,32] When account of fluctuations of doping impurity concentrations, the distribution of the density of states versus the energy E in the conduction band is represented in the form [33]

$$\rho_c(E) = \frac{m_c}{2\pi\hbar^2 N_p} \sum_n \sum_\nu \operatorname{erfc}\left(\frac{E_{c0} + E_{cn\nu} - E}{\sigma_c}\right), \tag{13}$$

where σ_c is the characteristic parameter of the tail of the density of electron states. Similar expression is obtained for the distribution of the density of holes states $\rho_v(E)$ with the characteristic tail parameter σ_v.

In doping superlattices, electron and hole quantum wells are spatially removed and, therefore, the fluctuations of impurity concentrations in different doped regions are independent. The tail parameters are determined by average values of the donor and acceptor concentrations N_d and N_a and by the screening lengths L_e and L_h in n- and p-regions, respectively. The expressions for the tail parameters have the form [29,31,32]

$$\sigma_c = \frac{e^2}{\epsilon}\sqrt{4\pi N_d L_e}, \quad \sigma_v = \frac{e^2}{\epsilon}\sqrt{4\pi N_a L_h}. \tag{14}$$

Here the screening lengths in n- and p-regions of the superlattice can be evaluated in the two-dimensional electron gas limit as follows [34]

$$\frac{1}{L_e} = \frac{2\pi e^2}{\epsilon} \cdot \frac{dn}{d\eta_c}, \quad \frac{1}{L_h} = \frac{2\pi e^2}{\epsilon} \cdot \frac{dp}{d\eta_v}, \tag{15}$$

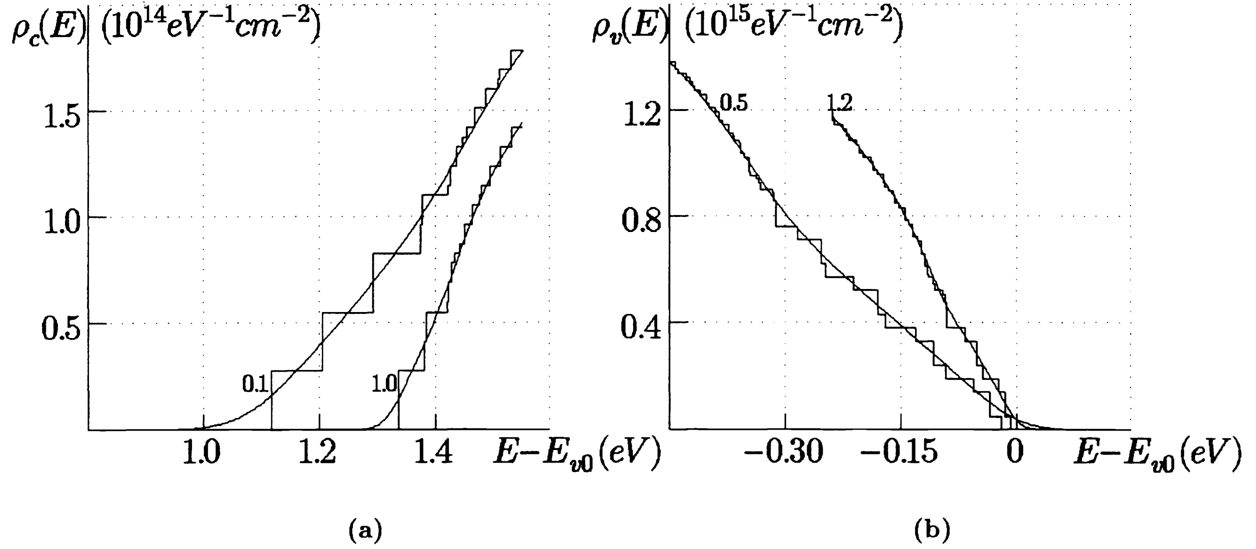

Fig. 9. Distributions of the density of states in (a) conduction and (b) valence bands at the different pump factors r (numbers at the curves) without (step curves) and with taking into account the density state tails (smooth curves). (a) $N_a = 10^{19}$ cm^{-3}, $N_d = 6 \times 10^{18}$ cm^{-3}, $\sigma_c = 93$ meV, $E_g^{'} = 1.08$ eV at $r = 0.1$ and $\sigma_c = 37$ meV, $E_g^{'} = 1.32$ eV at $r = 1.0$, (b) $N_a = 6 \times 10^{18}$ cm^{-3}, $N_d = 10^{19}$ cm^{-3}, $\sigma_v = 55$ meV, $E_g^{'} = 1.08$ eV at $r = 0.5$ and $\sigma_c = 21$ meV $E_g^{'} = 1.32$ eV at $r = 1.2$. $d_n = d_p = 15$ nm, $d_i = 0$, $N_p = 6$, $m_c = 0.066m_e$, $m_{vh} = 0.34m_e$, $m_{vl} = 0.093m_e$, $T = 300$ K.

where $\eta_c = F_e - E_{c0}$ and $\eta_v = E_{v0} - F_h$ are the chemical potentials for electrons and holes.

In the framework model, the self-consistent solution of the Schrödinger and Poisson's equations was numerically produced. Calculation examples of distributions of the density of states for electrons and holes in the GaAs n- and p-type doping superlattices are shown in Fig. 9. As seen, fluctuations of impurity concentrations smooth the ideal step-like distributions. Increasing the excitation pump leads to the decrease of the screening lengths and, accordingly, shortening the tails of the density of states.

3.2. Screening and the diffusivity - mobility ratio

The relation between the diffusion coefficient D and mobility μ of current carriers belongs to one from the most important thermodynamical parameters of semiconductors. The ratio D/μ attributes with the screening length, processes of diffusion and recombination, thermoelectric power, activity coefficient, photoconductivity, and time response of different optoelectronics semiconductor structures. [35] In some specific physical conditions and systems the diffusivity-mobility ratio D/μ exhibits abnormal behaviour in dependence on the concentration of carriers and temperature. Such systems include heavily doped semiconductor materials with impurity state bands [36] and screened density states tails, [32] as well as low-dimensional structures of quantum well layer or quantum wire types. [15,37] Doping superlattices is one more semiconductor system with abnormal character of the D/μ ratio.

Deformations of the energy spectrum in quantum wells of doping superlattices, because of high levels of doping with donors and acceptors, are reflected on the D/μ ratio. Standard relations between the diffusion coefficient and mobility for electrons in n-regions and for holes in p-regions of the superlattice have the form

$$\frac{D_n}{\mu_n} = \frac{n}{e} \cdot \frac{d\eta_c}{dn}, \quad \frac{D_p}{\mu_p} = \frac{p}{e} \cdot \frac{d\eta_v}{dp}. \tag{16}$$

Here the subscripts n and p correspond to n- and p-regions, respectively. The two-dimensional concentration, when taking into account the tail of the density of states, is determined by the expression

$$n = \frac{m_c}{2\pi\hbar^2 N_p} \sum_n \sum_\nu \left[-x_c \mathrm{erfc}\left(\frac{x_c}{\sigma_c}\right) + \exp\left(-\frac{x_c^2}{\sigma_c^2}\right) \left(\frac{\sigma_c}{\sqrt{\pi}} - kTF(\alpha_c, q_c)\right)\right], \tag{17}$$

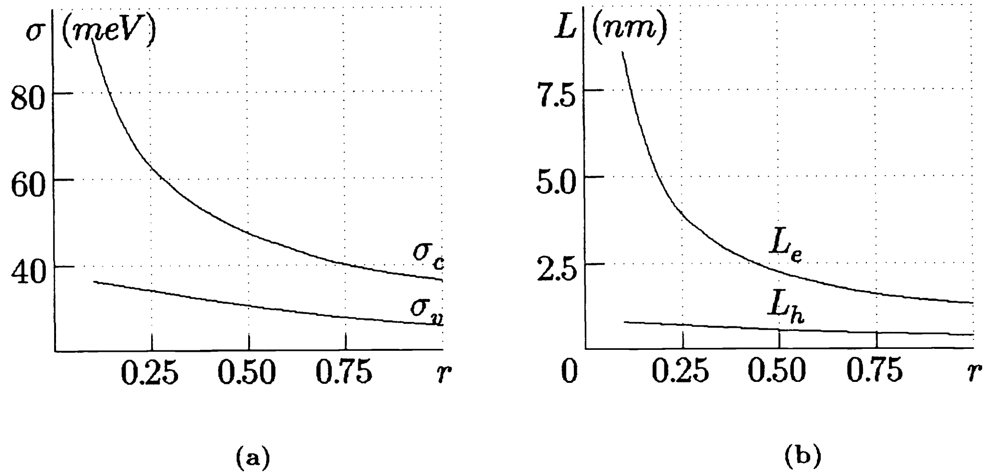

Fig. 10. (a) Parameters of density state tails $\sigma = \sigma_c$ or σ_v and (b) screening lengths $L = L_e$ or L_h in n- or p-regions, respectively, versus the pump factor r. $N_a = 10^{19}$ cm^{-3}, $N_d = 6 \times 10^{18}$ cm^{-3}, $d_n = d_p = 15$ nm, $d_i = 0$, $N_p = 6$, $T = 300$ K.

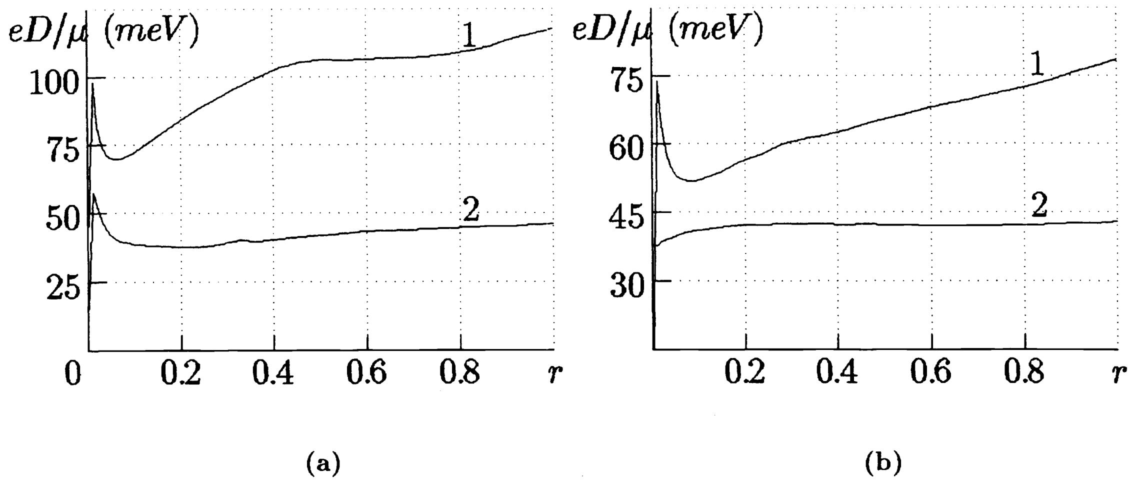

Fig. 11. Diffusivity-mobility ratio for (1) electrons and (2) holes versus the pump factor r. (a) $N_a = N_d = 10^{19}$ cm^{-3}, (b) $N_a = 10^{19}$ cm^{-3}, $N_d = 5 \times 10^{18}$ cm^{-3}. $d_p = d_n = 15$ nm, $d_i = 0$, $T = 300$ K.

where $x_c = E_{c0} + E_{cn\nu} - F_e$, $\alpha_c = kT/\sigma_c$, $q_c = 2\alpha_c x_c/\sigma_c$. the function $F(\alpha_c, q_c)$ is represented by the sum

$$F(\alpha_c, q_c)=\sum_{k=1}^{\infty}\frac{(-1)^k}{k}\left[\exp\left(\frac{k+q_c}{2\alpha_c}\right)^2\operatorname{erfc}\left(\frac{k+q_c}{2\alpha_c}\right)+\exp\left(\frac{k-q_c}{2\alpha_c}\right)^2\operatorname{erfc}\left(\frac{k-q_c}{2\alpha_c}\right)\right]. \tag{18}$$

It has maximum at the point $q_c = 0$ and is proportional to q_c^2. E.g., the function $F(\alpha_c, q_c)$ at $\alpha_c = 1$ can be approximately taken as $F(1, q_c) = -0.93 - 0.16q_c^2$.

When Eq. (17) is substituted into Eq. (16), the following relation between the diffusion coefficient and mobility of electrons been in n-regions of the n-i-p-i crystal is fulfilled

$$e\frac{D_n}{\mu_n} = \frac{\sum\limits_{n}\sum\limits_{\nu}\left[-x_c\operatorname{erfc}\left(\frac{x_c}{\sigma_c}\right)+\exp\left(-\frac{x_c^2}{\sigma_c^2}\right)\left(\frac{\sigma_c}{\sqrt{\pi}}-kTF(\alpha_c, q_c)\right)\right]}{\sum\limits_{n}\sum\limits_{\nu}\left[\operatorname{erfc}\left(\frac{x_c}{\sigma_c}\right)+\exp\left(-\frac{x_c^2}{\sigma_c^2}\right)R(\alpha_c, q_c)\right]}. \tag{19}$$

Here, the sum

$$R(\alpha_c, q_c) = \sum_{k=1}^{\infty}(-1)^k\left[\exp\left(\frac{k+q_c}{2\alpha_c}\right)^2\operatorname{erfc}\left(\frac{k+q_c}{2\alpha_c}\right)-\exp\left(\frac{k-q_c}{2\alpha_c}\right)^2\operatorname{erfc}\left(\frac{k-q_c}{2\alpha_c}\right)\right] \tag{20}$$

equals to 0 at $q_c = 0$. By analogy with Eq. (19) an expression which connects the ratio D_p/μ_p for holes with the tail parameter σ_v and screening length L_h in p-regions of the superlattice is apparently written.

Results of the calculations for the GaAs structures are shown in Figs. 10 and 11. For the p-type doping superlattice, the screening length and tail parameter for electrons are higher than for holes . At increasing the pump factor $r = n/N_d d_n$ the screening lengths decrease and the tails of the density of states become shorter.

The initial growth of the D/μ ratio versus r is caused by the quasi-Fermi level shift in the region of the density state tails. The following abnormal change of the D/μ ratio is conditioned by shortening the tails due to the effect of screening by nonequilibrium current carriers. For compensated superlattices, decrease of D/μ at increasing r occur for both electrons and holes. In the p-type superlattices, abnormal behaviour in D/μ takes place only for electrons. In this case, the density tails in n-regions shorten the most strongly. The values of L_e and L_h are found to be smaller as compared with the superlattice period. Therefore, the screening of the fluctuated impurity charge potential in doping superlattices is actually accomplished by current carriers only of a certain type, i.e., by electrons in n-regions and by holes in p-regions.

4. LIGHT EMISSION CHARACTERISTICS

4.1. Spectra of spontaneous emission and gain

Radiative recombination and absorption (gain) spectra in doping superlattices depend on the variation of the potential relief under excitation and accordingly on changed overlap integrals of envelope wave functions of electrons and holes in the subbands. [24] In particular, the coefficient of absorption for isotropic radiation is given as follows

$$\begin{aligned} K(\nu) &= \frac{A_{cv}}{\pi\hbar^2 v\rho d N_p}\left[exp\left(\frac{h\nu-\Delta F}{kT}\right)-1\right] \\ &\times \sum_i m_{ri}\sum_n\sum_m\sum_\nu f_e\left(E_{cnmi\nu}\right)f_h\left(E_{vmin\nu}\right)I^2_{nmi\nu}H_{nmi\nu}. \end{aligned} \tag{21}$$

Here, A_{cv} is the Einstein coefficient, ρ is the density of electromagnetic modes, v is the light velocity in the crystal. The distribution functions have the form

$$\begin{aligned} f_e\left(E_{cnmi\nu}\right) &= \left(1+exp\frac{E_{cnmi\nu}-F_e}{kT}\right)^{-1}, \\ f_h\left(E_{vmin\nu}\right) &= \left(1+exp\frac{F_h-E_{vmin\nu}}{kT}\right)^{-1}, \end{aligned} \tag{22}$$

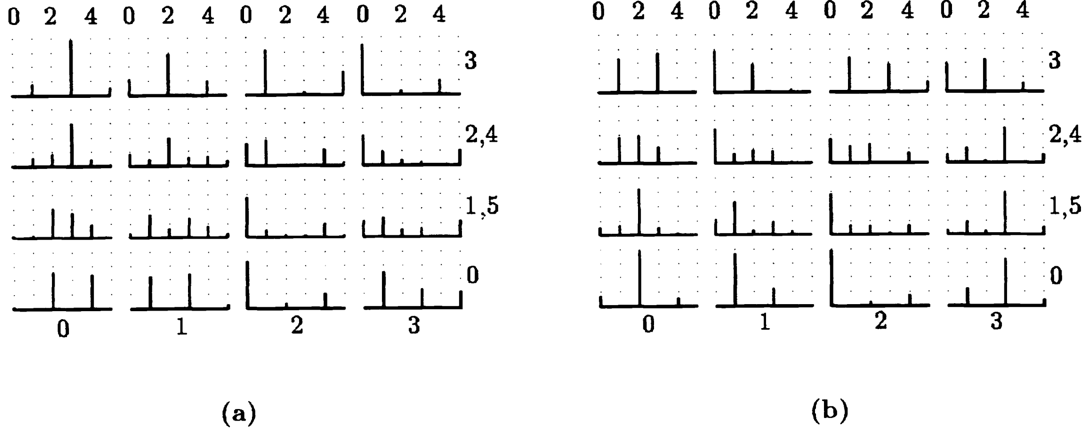

Fig. 12. Squared overlap integrals $I^2_{nml\nu}$ at (a) $r \approx 0$ and (b) $r = 0.5$ for transitions between electron subbands with the quantum numbers n (the bottom figures) and light hole subbands with the quantum numbers m (the upper figures) with different quantum numbers of minisubbands ν (the figures on the right). The values of $I^2_{nml\nu}$ are given in the unit scale. $N_a = 10^{19}$ cm^{-3}, $N_d = 8 \times 10^{18}$ cm^{-3}, $d_n = d_p = 10$ nm, $d_i = 0$, $N_p = 6$.

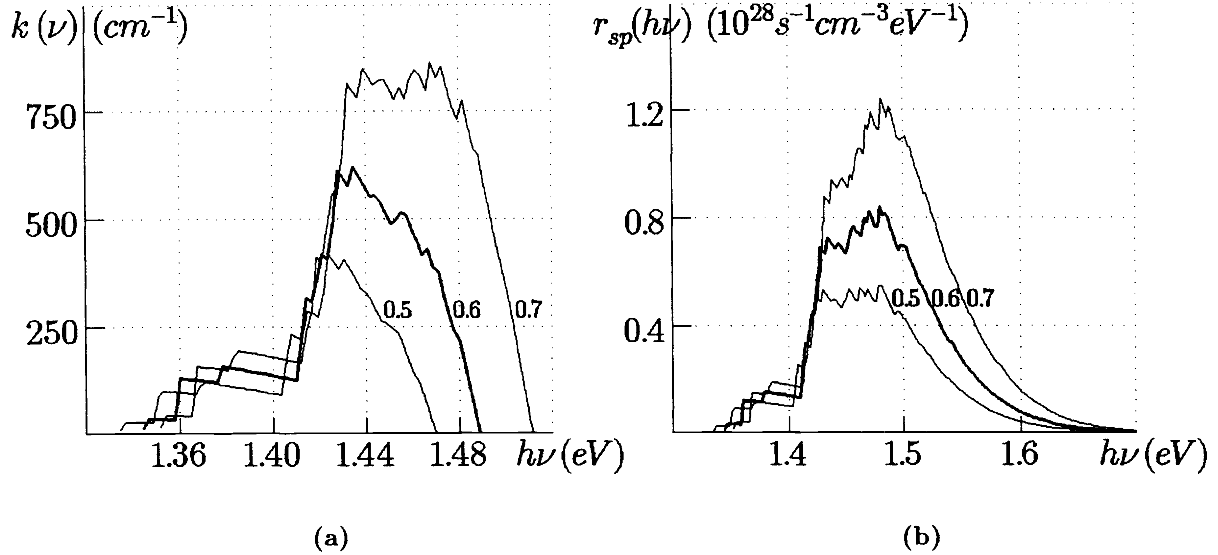

Fig. 13. (a) Gain and (b) emission spectra for different values of the pump factor r (numbers at the curves) in the GaAs doping superlattice. $N_a = 10^{19} cm^{-3}$, $N_d = 8 \times 10^{18} cm^{-3}$, $d_n = d_p = 10nm$, $d_i = 0$, $N_p = 6$, $T = 300K$.

where

$$E_{cnmi\nu} = E_{c0} + \frac{m_{ri}}{m_c}\left(h\nu - E_g^{'}\right) + \frac{m_{ri}}{m_{vi}}E_{cn\nu} - \frac{m_{ri}}{m_c}E_{vim\nu},$$
$$E_{vmin\nu} = E_{v0} - \frac{m_{ri}}{m_{vi}}\left(h\nu - E_g^{'}\right) + \frac{m_{ri}}{m_{vi}}E_{cn\nu} - \frac{m_{ri}}{m_c}E_{vmi\nu}, \quad (23)$$

$\Delta F = F_e - F_h$, $m_{ri} = m_c m_{vi}/(m_c + m_{vi})$ is the reduced mass. Transitions between the subbands begin from the light quanta $h\nu_{nmi\nu} = E_g^{'} + E_{cn\nu} + E_{vmi\nu}$. Because of this, in Eq.(21) appears the Heaviside unit step function $H_{nmi\nu}$ with the magnitudes of $H_{nmi\nu} = 1$ at $h\nu \geq h\nu_{nmi\nu}$ and $H_{nmi\nu} = 0$ at $h\nu < h\nu_{nmi\nu}$. The summation is made with respect to the quantum numbers n, m, ν and the states of heavy and light holes. The overlap integral of the wave functions of electrons and holes is determined as

$$I_{nmi\nu} = \int_0^d \psi^*_{vim\nu}\psi_{cn\nu}dz. \quad (24)$$

Increased overlap integrals values can be obtained in δ-doped structures. The use of δ-doped layers makes it possible to attain considerable changes in the depth of modulation of the potential relief and introduce high concentrations of impurities for the photosensitive and light emitting structure optimization. The sheet concentration of impurities was brought up to 2×10^{13} cm^{-2}, for example, when doping GaAs with the donors Si and acceptor impurity Be to create laser structure. [38] In this case, the potential relief deep modulation is reached together with shortening the superlattice period, the energy separation between subbands increases, and influence of random distribution of dopants on the states of carriers and on their energy and momentum relaxation is reduced.

A new structure consisting of alternating n-type doped layers and p-type δ-doped sheets separated by intrinsic semiconductor layers was proposed in Ref. 25. The modified structure permits to increase overlap integrals values because of the quasi-parabolic quantum wells for electrons have width larger than widths for sawtooth-like hole quantum wells.

As an example, in Fig. 12, squared overlap integrals values are represented for a typical *GaAs* six-period doping superlattice. Probability of transitions between different is determined by the parity of the overlapping envelope wave functions both within potential wells and in the space between wells. In addition, the selection rule in respect to the quantum numbers of minisubbands ν. The wave function parity depends on the quantum numbers ν, i.e., on electron and hole wave vectors along the z-axis of the superlattice.

It has an effect on the intensity and shape of the spontaneous and stimulated emission spectra (Fig. 13). The rate of transitions at spontaneous recombination $r_{sp}(h\nu)$ can be found using the universal relation between radiative recombination and absorption, i.e.,

$$r_{sp}(h\nu) = \frac{v\rho}{exp\left(\frac{h\nu - \Delta F}{kT}\right) - 1}K(\nu). \quad (25)$$

In its turn, the gain equals to the absorption coefficient with the negative sign and is reached when $\Delta F > h\nu$. The gain coefficient $k(\nu) = -K(\nu)$ in the maximum can be obtained up to 10^3 cm^{-1}.

4.2. Laser parameters

Laser structures based on doping superlattices are of interest because they provide a means for tuning the lasing spectrum over a wide range. A high doping level in the superlattice structures requires the consideration of the violation of the k-selection rule for electron transitions at the analysis of spectral and other characteristics. In this case, the model with no the k-selection rule is used for description of characteristics and parameters of quantum-well laser system. [15,39] It is also necessary to account that the probability of optical transitions becomes to decrease at sufficiently small widths of quantum wells. [40]

To determine laser parameters of doping superlattices, a simplified approach in the model with no the k-selection rule was applied. [41] The rate of spontaneous emission recombination is represented in the following form

$$r_{sp}(h\nu) = \frac{A}{d}\int_0^d \int_{E_{c0}+E_{c00}}^{E_{v0}(z)+h\nu} \sum_n \sum_\nu |\psi_{cn\nu}(z)|^2 \rho_{cn\nu}(E)$$
$$\times \rho_v(E - h\nu, z) f_e(E) f_h(E - h\nu)\, dE\, dz. \quad (26)$$

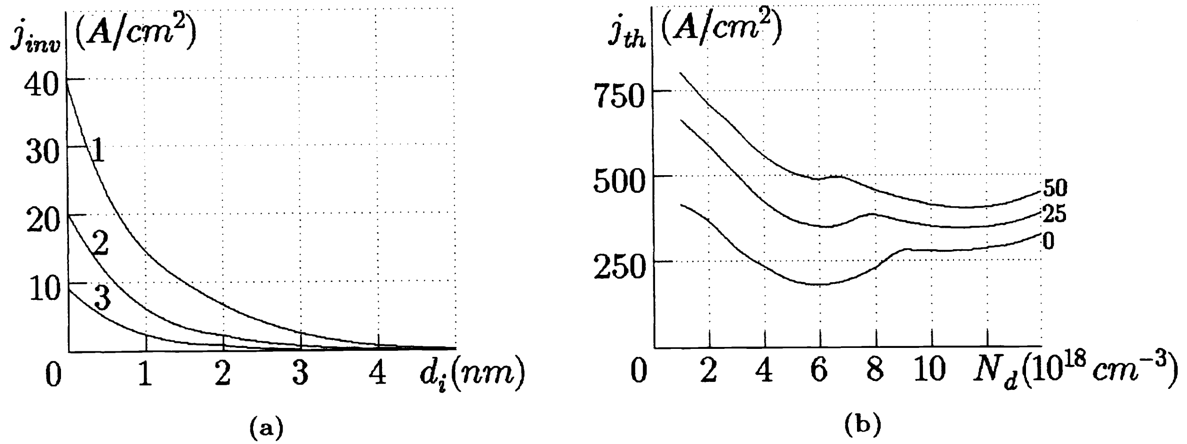

Fig. 14. (a) Dependence of the inversion current density j_{inv} on the thickness of intrinsic layers d_i at different concentrations of donor impurities (1) $N_d = 5 \times 10^{18}$ cm^{-3}, (2) $N_d = 6 \times 10^{18}$ cm^{-3}, and (3) $N_d = 7 \times 10^{18}$ cm^{-3}. $N_a = 10^{19}$ cm^{-3}, $d_n = d_p = 10$ nm, $T = 300$ K. (b) Dependence of the threshold current density on correlation between donor and acceptor concentrations. Numbers at the curves are cavity losses (cm^{-1}) excluding free carriers absorption $N_a = 7 \times 10^{18}$ cm^{-3}, $d_n = d_p = 10$ nm, $d_i = 0$, $T = 300$ K.

Here, $A = 32\pi a_0^3 A_{cv}$ is the probability of optical transitions with no the k-selection rule, a_0 is the effective Bohr radius of impurities, f_e and f_h are the distribution functions for electrons and holes. In the electron band the two-dimensional density of states for a minisubband with the quantum numbers n, ν has the form

$$\rho_{cn\nu}(E) = \frac{m_c}{\pi\hbar^2 N_p} H(E - E_{c0} - E_{cn\nu}), \tag{27}$$

where E is the energy of levels participating in the transitions, $H(E)$ is the Heaviside unit step function. The quantity $\rho_v(E, z)$ is the density of states in the impurity band overlapping with the valence band edge. Without regard for the tail of the density of states, the first approximation to $\rho_v(E, z)$ can be assumed to be the volume density of states

$$\rho_v(E, z) = \frac{(2m_v)^{3/2}}{2\pi^2\hbar^3} \left(E_{v0}(z) - E\right)^{1/2}, \tag{28}$$

where m_v is the hole density effective mass, the energy $E_{v0}(z)$ follows the superlattice potential relief along the z-axis. The total recombination rate is evaluated by the integrating of Eq. (26) over all energies of emitted photons and is equal to

$$R_{sp} = \frac{A}{d} \int_0^d n(z) p_v(z) dz, \tag{29}$$

where $p_v(z)$ is the volume concentration of holes depending on the z-coordinate of the potential relief.

Among important laser parameters there are inversion and zero currents, gain factor, internal optical losses, and quantum efficiency. The inversion current gives the minimum value of the laser threshold. This value is determined in conditions where the difference of the quasi-Fermi levels for electrons and holes ΔF reaches the minimum energy of emitted quanta $h\nu_{min}$ which is related to the effective energy band gap of the superlattice. The last characteristic can be varied through the choice of the concentrations of donors N_d and acceptors N_a and the thicknesses d_n, d_p, and d_i of n-, p-, and i-layers. Assuming that the injection efficiency and quantum yield of luminescence are close to 1, for the inversion current density per a period of the superlattice one has

$$j_{inv} = edR_{sp}|_{\Delta F = h\nu_{min}}. \tag{30}$$

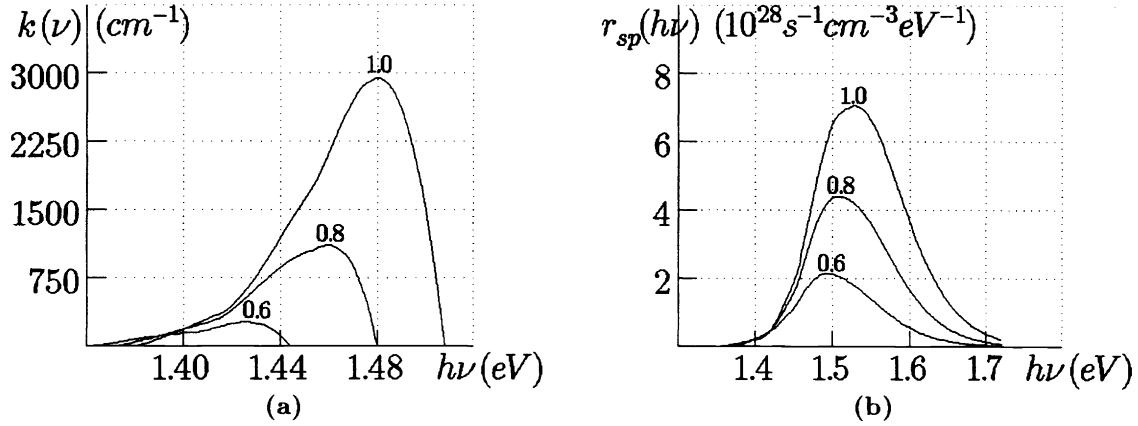

Fig. 15. (a) Gain and (b) emission spectra for different values of the pump factor r (numbers on the curves). $N_a = 10^{19}$ cm^{-3}, $N_d = 7 \times 10^{18}$ cm^{-3}, $d_p = d_n = 10$ nm, $d_i = 0$, $T = 300K$, $a_0 = 1.7$ nm, $A_{cv} = 1.5 \times 10^9$ c^{-1}, $A = 8 \times 10^{-10}$ c^{-1}cm^3.

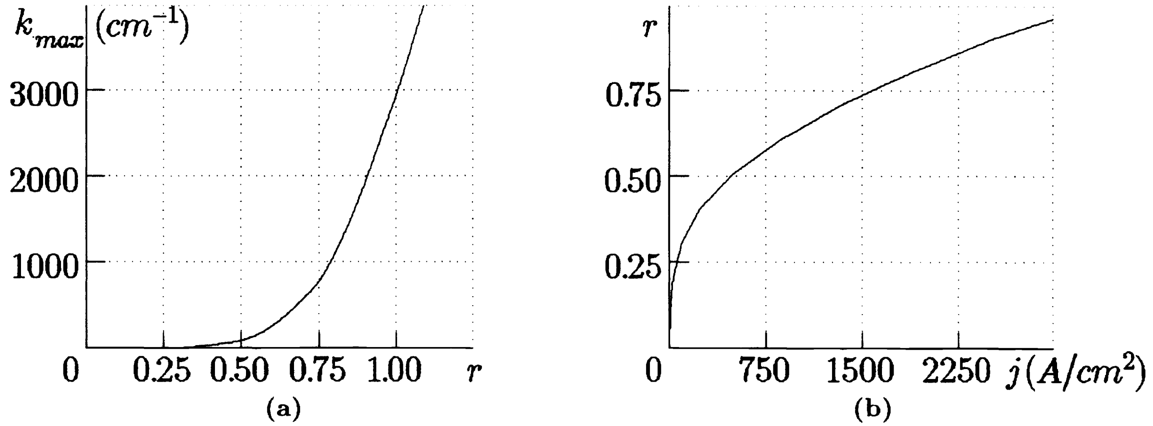

Fig. 16. (a) Dependence of the maximum gain coefficient k_{max} on the pump factor r and (b) the relation $r(j)$. $N_a = 10^{19}$ cm^{-3}, $N_d = 7 \times 10^{18}$ cm^{-3}, $d_p = d_n = 10$ nm, $d_i = 0$, $T = 300$ K.

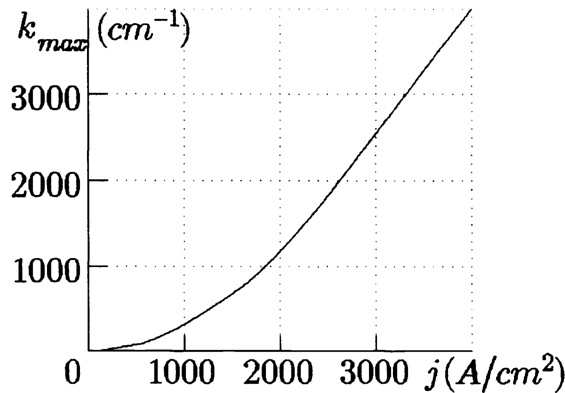

Fig. 17. Dependence of the maximum gain coefficient k_{max} on the current density j. $N_a = 10^{19}$ cm^{-3}, $N_d = 7 \times 10^{18}$ cm^{-3}, $d_p = d_n = 10$ nm, $d_i = 0$, $T = 300$ K.

Calculations were performed in the GaAs system. The parameter j_{inv} versus the thickness d_i is shown in Fig. 14 (a). The inversion current density decreases with increasing the superlattice period because of increasing spatial separation of electrons and holes. Due to small oscillator strengths of optical transitions, the inversion current density values do not exceed several tens A/cm^2.

Influence of the doping level on the threshold current was calculated taking into account free carriers absorption. Estimation of the absorption includes contributions of scattering processes involving ionized impurities, acoustic and optical phonons. [42] The main canal of the absorption is intrasubband electron transitions in n-regions. As seen, from Fig. 14(b), the threshold current density j_{th} per a superlattice period can be optimized by choice of donor and acceptor concentrations. At low losses, optimized laser structures correspond to p-type doping superlattices. But, when increasing the cavity losses, the minimum threshold is reached in n-type structures.

The gain and emission spectra have been calculated and their transformation with pump are represented in Fig. 15. The level of excitation of the structure can be described by the factor $r = n/N_d d_n$, where n is the two-dimensional concentration of electrons. The gain coefficient $k(\nu)$ is determined from Eq. (26) according to the standard relation between the spontaneous emission recombination rate and absorption (gain) coefficient (Eq. (25)). It is seen that the maximum value of the gain coefficient k_{max} reaches up to 10^3 cm^{-1} at room temperature.

To find the internal laser parameters, consider results in Fig. 16. If k_{max} is above 400 cm^{-1}, the dependence of k_{max} on r can be approximately described by a linear function $k_{max} = \kappa(r - r_0)$. Here, the zero pump factor $r_0 \approx 0.6$ and $\kappa \approx 7000$ cm^{-1} for the structure under study. Using the relation between r and n, the differential gain $g = \partial k_{max}/\partial n$ can be estimated. For the examined laser superlattice the value of g is about 10^{-9} cm. The two-dimensional concentration of nonequilibrium current carriers corresponding to the zero pump conditions reaches 4.2×10^{12} cm^{-2}.

In general, the dependence of the gain on the injection current in the doping superlattices is nonlinear in a wide interval of k_{max} (Fig. 17). But, in the practical important interval of the gain values $1000 - 3000$ cm^{-1}, an ordinary linear function $k_{max} = \beta(j - j_0)$ gives a good fitting for the gain behaviour versus pump. For the structure under study, it was obtained $j_0 \approx 1100$ A/cm^2 and $\beta \approx 1.4$ cm/A. These values correspond to a period of the superlattice. The performed calculations of the internal parameters permit to optimize laser n-i-p-i structures.

5. CONCLUSION

Analysis of obtained results at investigations of optical and electric properties and characteristics of doping superlattices (n-i-p-i crystals) lead to the following conclusions. (a) Doping superlattices is a new class of tunable semiconductor structures. (b) Modifications due to δ-doping or additional incorporated quantum wells widen functions of the structures. (c) Laser parameters can be optimized by choice of doping impurity concentrations and the structure design. For the GaAs superlattices the maximum gain exceeds 10^3 cm^{-1} at room temperature and depends practically linearly on the injection current. For further improvement of laser characteristics it is necessary to select waveguide parameters and an optimal number of superlattice periods. (d) High optical nonlinear response is achieved at low excitation powers about some mW/cm^2. (e) Screening and transport processes in doping superlattices have some peculiarities in comparison with ordinary bulk semiconductor structures. In particular, the diffusivity-mobility ratio prohibits abnormal behaviour. (f) Some questions concerning of high level of impurity concentrations, details of mechanisms of transport, relaxation, and recombination of carriers, time response, collective charge phenomena, exciton formation, absorption by free carriers remain still.

6. ACKNOWLEDGMENT

The work was supported by the Belarussian Republican Foundation for Fundamental Research.

7. REFERENCES

[1] L.V. Keldysh, " Effect of ultrasound on the electron spectrum of a crystal ", Sov. Phys.-Solid State 4(8), 2265-2267 (1962).

[2] L. Esaki and R. Tsu, " Superlattice and negative differential conductivity in semiconductors ", IBM J. Res. Develop. 14(1), 61-65 (1970).

[3] M.I. Ovsyannikov, Yu.A. Romanov, V.N. Shabanov, and R.G. Loginova, " Periodic semiconductor structures ", Sov. Phys.- Semicond. 4(12), 2225-2231 (1970).

[4] A.E. Blakeslee and C.F. Aliotta, " Man-made superlattice crystals ", IBM J. Res. Develop. **14**(6), 686-688 (1970).

[5] G.I. Alferov, Yu.V. Zhilyaev, and Yu.V. Shmartsev, " Splitting of the conduction band in a "superlattice" based on GaP_xAs_{1-x} ", Sov. Phys.- Semicond. **5**(1), 196-198 (1971).

[6] G.H. Döhler, " Electron states in crystals with "nipi- superstructure" ", Phys. stat. sol. (b) **52**(1), 79-92 (1972).

[7] L.L. Chang, L. Esaki, W.E. Howard, and R. Ludeke, " The growth of a GaAs-AlGaAs superlattice ", J. Vac. Sci. Technol. **10**(1), 11-16 (1973).

[8] K. Ploog, A. Fischer, and H. Künzel, " The use of Si and Be impurities for novel periodic doping structures in GaAs grown by molecular beam epitaxy ", J. Electrochem. Soc. **128**(2), 400-410 (1981).

[9] E.F. Schubert, A. Fischer, Y. Horikoshi, and K.Ploog, " GaAs sawtooth superlattice laser emitting at wavelengths $\lambda > 0.9\mu m$ ", Appl. Phys. Lett. **47**(3), 219-221 (1985).

[10] G.H. Döhler, J.N. Miller, R.A. Street, and P.P. Ruden, " Investigation of luminescence and non-linear optical properties of hetero n-i-p-i superlattices", Surface Sci. **174**(1-3), 240-247 (1986).

[11] H. Ando, H. Iwamura, H. Oohashi, and H.Kanbe, " Nonlinear absorption in n-i-p-i MQW structures ", IEEE J. Quantum Electron. **25**(10), 2135-2141 (1989).

[12] K. Ploog and G.H. Döhler, " Compositional and doping superlattices in III-V semiconductors ", Adv. Phys. **32**(3), 285-359 (1983).

[13] A.P. Silin, " Semiconductor superlattices ", Sov. Phys.-Usp. **147**(3), 485-521 (1985).

[14] G.H.Döhler, " Doping superlattices (" n-i-p-i crystals ") ", IEEE J. Quantum Electron **QE-22**(9), 1682-1694 (1986).

[15] V.K. Kononenko, Optical Properties of Heterostructures with Quantum Size Layers, Preprint (492), IP AS BSSR, Minsk (1987).

[16] G.H. Döhler, " n-i-p-i and hetero n-i-p-i doping superlattices physics and device applications ", Proc. SPIE **1523**, 23-63 (1992).

[17] V.K. Kononenko, " Spectral characteristics of quantum-well heterolasers ", Proc. SPIE **1724**, 89-101 (1992).

[18] D. Teng, Y.H. Lo, C.H. Lin, and L.F. Eastman, " Effects of nonuniform well width on compressively strained multiple quantum well lasers ", Appl. Phys. Lett. **60**(22), 2729-2731 (1992).

[19] V.K. Kononenko, I.S. Manak, S.V. Nalivko, V.A. Shevtzov, and D.S. Shulyaev, " Gain and luminescence spectra of broad-band sources based on asymmetric quantum-well heterostructures ", J. Appl. Spectrosc. **64**(2), 221-227 (1997).

[20] A.M. Glass, E.F. Schubert, B.A. Wilson, C.E. Bonner, J.E. Cunningham, D.H. Olson, and W. Jan, " Novel photovoltaic δ-doped GaAs superlattice structure ", Appl. Phys. Lett. **54**(23), 2318-2320 (1989).

[21] E.F. Schubert, " Optical and electronic properties of delta-doped doping supelattices ", Opt. Quantum Electron **22**, S141-S186 (1990).

[22] S.E. Ralph, F. Capasso, and R.J. Malik, " New photorefractive effect in graded-gap superlattices ", Phys. Rev. Lett. **63**(20), 2272-2275 (1989).

[23] G.H. Döhler, H. Künzel, and H. Ploog, " Tunable absorption coefficient in GaAs doping superlattices ", Phys. Rev. B **25**(4), 2616-2626 (1982).

[24] D.V. Ushakov, V.K. Kononenko, I.S. Manak, and V.A. Shevtzov, " Energy levels and absorption and emission spectra of n-i-p-i crystals ", Advances in Synergetics **8**, 343-351, Minsk (1997).

[25] D.V. Ushakov and V.K. Kononenko, " Variation of the potential relief and emission spectra in doping superlattices under excitation ", Physics, Chemistry, and Application of Nanostructures, 121-124, Singapore (1997).

[26] P. Ruden and G.H. Döhler, " Electronic structure of semiconductors with doping superlattices ", Phys. Rev. B **27**(6), 3538-3546 (1983).

[27] S. Das Sarma, R. Jalabert, and S.-R.E. Yang, " Band-gap renormalization in semiconductor quantum wells ", Phys. Rev. B **41**(12), 8288-8294 (1990).

[28] A. Chavez-Pirson, O. Vatel, M. Tanimoto, H. Ando, H. Iwamura, and H. Kanbe, " Nanometer-scale imaging of potential profiles in optically excited n-i-p-i heterostructure using Kelvin probe force microscopy ", Appl. Phys. Lett. **67**(21), 3069-3071 (1995).

[29] B.I. Shklovskii and A.L. Efros, Electronic Properties of Doped Semiconductors, Moscow (1979).

[30] H.J. Beyer, C. Metzner, J. Heitzer, and G.H. Döhler, " Temperature dependence of the tunable luminescence, absorption and gain spectra of nipi doping superlattices – theory and comparison with experiment ", Superlattices and Microstructures **6**(3), 351-356 (1989).

[31] E.O. Kane, " Thomas-Fermi approach to impure semiconductor band structure ", Phys. Rev. **131**(1), 79-88 (1963).
[32] V.K. Kononenko, Charge Transport and Screening in Heavily Doped Semiconductors, Preprint (224), IP AS BSSR, Minsk (1980).
[33] D.V. Ushakov, V.K. Kononenko, and I.S. Manak, " Influence of fluctuations of impurity concentrations on the energy spectrum of doping superlattices ", Proc. III Conf. on Laser Physics and Spectroscopy 1, 384-386, Grodno (1997).
[34] A.Ya. Shik, " Electrodynamics of two-dimensional electron systems ", Sov. Phys.-Semicond. **29**(8), 1345-1381 (1995).
[35] K.P. Ghatak and M. Mondal, " The diffusivity-mobility ratio in nonparabolic materials ", J. Appl. Phys. **71**(8), 1277-1283 (1992).
[36] V.K. Kononenko, " On relation between the diffusion coefficient and mobility for heavily doped semiconductors ", J. Appl. Spectrosc. **23**(2), 357-358 (1975).
[37] V.K. Kononenko, " Relation between the diffusion coefficient of electrons and mobility in structures with quantum-size confinement ", Abstr. VI Union Symp. on Plasma and Instabilities in Semiconductors, 138-139, Vilnius (1986).
[38] E.F. Schubert, " Optical properties of δ-doped doping superlattices ", Surface Sci. **228**(1-3), 240-246 (1990).
[39] V.K. Kononenko and I.S. Zakharova, Laser Parameters of Quantum-Well Heterostructures, Preprint (IC/93/63), ICTP, Trieste (1993).
[40] A.A. Afonenko, V.K. Kononenko, and I.S. Manak, " Gain spectra and optical transition probability in doped quantum-well heterostructures ", Proc. SPIE **2994**, 825-833 (1997).
[41] D.V. Ushakov and V.K. Kononenko, " Laser parameters of n-i-p-i crystals ", Abstr. 2nd GR-I Int. Conf. on New Laser Technologies and Applications, 175, Olympia (1997).
[42] K.V. Shalimova, Physics of semiconductors, Moscow (1985).

Prior to the PST conference beginning an opening ceremony of the exhibition: "MEDICA-LABORATORIUM and CONTROLA-OPTICA" was initiated by Teresa Ochmańska, Chair of M-L&C-O and Deputy-Director, Biuro Reklamy S. A., Warsaw, Poland (see the PST Chair's *Welcome Address* for some information on the M-L&C-O exhibition).